

# Sunshine to Rainstorm: Cross-Weather Knowledge Distillation for Robust 3D Object Detection

Xun Huang<sup>1\*</sup>, Hai Wu<sup>1\*</sup>, Xin Li<sup>2</sup>, Xiaoliang Fan<sup>1</sup>, Chenglu Wen<sup>1†</sup>, Cheng Wang<sup>1</sup>

<sup>1</sup> Xiamen University, <sup>2</sup> Texas A & M University  
 {huangxun,wuhai}@stu.xmu.edu.cn, {clwen, fanxiaoliang, cwang}@xmu.edu.cn, xinli@tamu.edu

## Abstract

LiDAR-based 3D object detection models inevitably struggle under rainy conditions due to the degraded and noisy scanning signals. Previous research has attempted to address this by simulating the noise from rain to improve the robustness of detection models. However, significant disparities exist between simulated and actual rain-impacted data points. In this work, we propose a novel rain simulation method, termed DRET, that unifies **D**ynamics and **R**ainy **E**nvironment **T**heory to provide a cost-effective means of expanding the available realistic rain data for 3D detection training. Furthermore, we present a **S**unny-to-**R**ainy **K**nowledge **D**istillation (**SRKD**) approach to enhance 3D detection under rainy conditions. Extensive experiments on the Waymo-Open-Dataset show that, when combined with the state-of-the-art DSVT model and other classical 3D detectors, our proposed framework demonstrates significant detection accuracy improvements, without losing efficiency. Remarkably, our framework also improves detection capabilities under sunny conditions, therefore offering a robust solution for 3D detection regardless of whether the weather is rainy or sunny.

## Introduction

Recent years have witnessed growing research interest in 3D object detection utilizing point cloud data. For widespread application in autonomous driving, such models must demonstrate robust performance under diverse conditions. Despite progress in 3D object detection on benchmark datasets, achieving consistent and reliable performance, particularly under adverse weather conditions (e.g., rain) remains an open challenge.

Unfortunately, 3D object detection research under rainy weather presents significant challenges at both the data and methods levels. At the data level, a pressing issue is data scarcity. Extant datasets exhibit highly limited rainy samples owing to the high annotation and collection costs. For instance, merely 0.6% of samples in the Waymo Open Dataset (WOD) [34] perception subset in rain. This shortage seriously hinders the research on 3D object detection under rainy weather. The low quality of rainy data obstructs 3D detectors. Analysis of rainy point clouds in the WOD reveals

\*These authors contributed equally.

†Corresponding author.

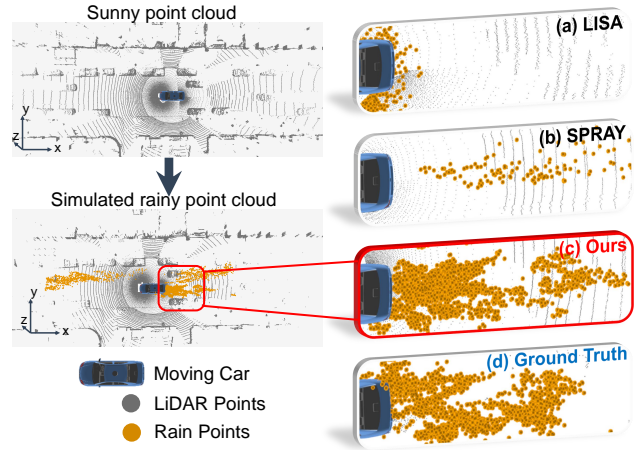


Figure 1: Visualization of rain noise points in groundtruth and different rain simulations.

two critical phenomena: 1) *Dense rain noise*. As LiDAR light pulses cannot penetrate water particles [11], resulting in noise from water droplets generated by moving vehicles. 2) *Missing points*. Atmospheric parameters like attenuation substantially differ in rain. Thus, many points fall below the LiDAR intensity threshold and are missed. These phenomena create a considerable domain gap between sunny and rainy data. Robust rainy 3D object detection needs to address both data and model challenges.

Prior work, including LISA [13] and SPRAY [29], has sought to address the challenge of insufficient training data by simulating adverse weather conditions. While these approaches are valuable, they overlook the rainy environmental theory and object-scene dynamics, leading to limitations in the realism of simulated rain. For example, as depicted in Fig. 1, a significant gap exists between simulated and real rain points, especially in the case of LISA. SPRAY also fails to simulate the phenomenon of missing points that usually occur in rainy scenes.

In addition to creating realistic simulations, the effective utilization of simulated data is also crucial. Many existing methods [23, 11, 26] simply augment training data with simulations, but this approach often falls short in adapting detectors effectively to new rainy environments. LDNet [37] designed an innovative idea of knowledge distillation from

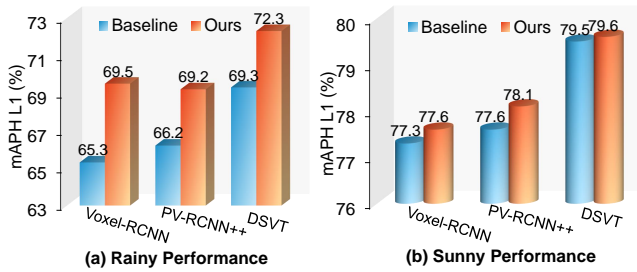


Figure 2: Comparison of the performance under both sunny and rainy weather conditions on the WOD.

sunny to severe weather conditions. Without a realistic rain simulation, this concept cannot be effectively applied. Moreover, LDNet also overlooks the data disparities between different weather conditions. Only by fully addressing the gaps between rainy and sunny weather can models achieve robustness across diverse weather conditions.

To enhance the robustness of models in rain, we propose innovative approaches at both the data and model levels. We introduce DRET, a method that unifies **D**ynamics and **R**ainy **E**nvironment **T**heory to create realistic rain data simulations. We also present SRKD, a **S**unny-to-**R**ainy **K**nowledge **D**istillation framework specifically tailored for 3D detectors in rainy conditions. SRKD trains a student network to learn from a sunny teacher detector, distilling knowledge of the same scene under rainy weather. Additionally, we design a noise-aware prediction correction module to effectively handle the noise associated with rain.

Our framework is highly adaptable and can be easily integrated with various 3D detectors. As shown in Fig.2, extensive experiments on the WOD validated that DRET and SRKD enhance the rain robustness of all 3D detectors without sacrificing efficiency. Remarkably, they also improve detectors’ performance under sunny conditions, possibly due to their increased robustness to sparse objects.

Our contributions are : (1) We analyzed the impact of various phenomena on 3D object detection in rainy weather, and proposed a new method, DRET, for more realistic rain simulation in 3D object detection. (2) We designed SRKD, a generalized framework to address the challenges posed by weather disparities in straightforward sunny-to-rainy distillation. It can significantly improve the robustness of the 3D detector in rain without compromising efficiency. (3) We validated the effectiveness and universality of our proposed approach through extensive testing on the state-of-the-art model, DSVT [10], as well as other classical 3D detectors, including PV-RCNN++ and Voxel-RCNN.

## Related Work

**Simulation of rain.** Physics-based simulations [23, 26, 11, 13] have been explored to reproduce point clouds under adverse weather conditions such as snow and fog. These methods help alleviate the issue of data scarcity to some extent, but they are not fully effective in simulating rainy weather. For instance, LISA [13] employs a rain simulation algorithm that relies on LiDAR light scattering augmenta-

tion, but it overlooks the impact of dense rain noise in rainy conditions. SPRAY [29] uses dynamics to simulate the water splashing effect caused by vehicles in the rain, but it fails to accurately mimic the actual distribution of splashed water due to the absence of a well-grounded physical theory. Consequently, substantial discrepancies persist between these simulated rainy datasets and actual rainy conditions.

**3D object detection.** Current 3D object detection methods primarily focus on clear weather conditions and can be categorized into single-stage and two-stage approaches. Single-stage methods, such as SECOND [20], PointPillars [33], SA-SSD [19], and SE-SSD [21], utilize voxel-based sparse convolution or point-based set abstraction for feature extraction. In two-stage algorithms, Voxel-RCNN [33], SFD [22], and VirConv [32] employ voxel-based sparse convolution, while PointRCNN [16] and STD [30] use point-based set abstraction. Notably, PV-RCNN [17], CT3D [8], and PV-RCNN++ [18] combine voxel-based and point-based operations in the two-stage approach. DSVT [10] introduces an efficient and deployable 3D transformer backbone that achieves state-of-the-art performance on WOD. Knowledge distillation has been explored in 3D object detection, including SparseKD [27], which examines lightweight models, and other works [5, 6] attempting distillation from multimodal/multi-frame models to single-modal/single-frame models. However, these mainstream methods still lack robustness in rain.

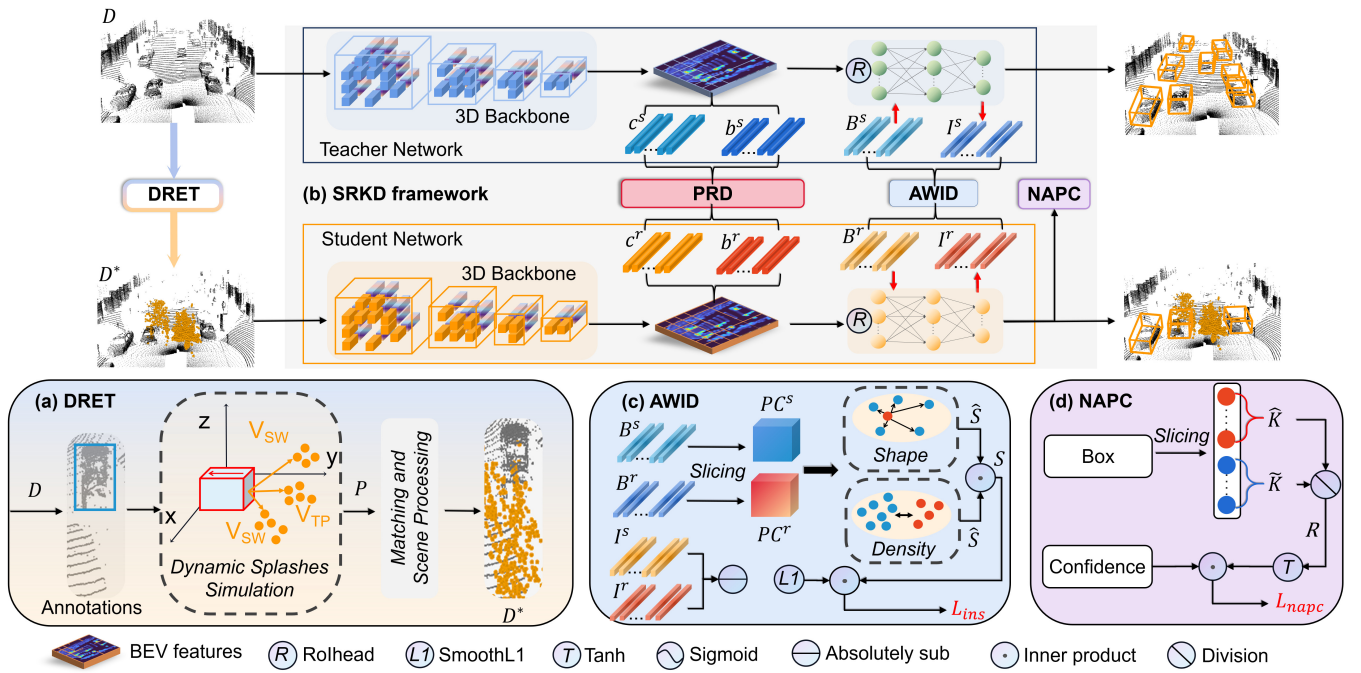
**3D object detection in adverse weather.** Recent studies, such as [9, 7], have introduced lightweight approaches that employ techniques like semantic segmentation or filtering algorithms to remove dense noise, thereby minimizing its impact on detection models. However, these methods heavily rely on the denoising model’s performance, leading to unstable detection results, and they do not account for the issue of missing points in rainy weather. [28] designed a general completion framework that addresses the problem of domain adaptation across different weather and environmental conditions. It achieves promising improvements on the WOD domain adaptation dataset, which contains a significant amount of rainy data. However, it solely focuses on the phenomenon of missing points, disregarding the impact of other phenomena.

## Method

The challenges associated with data limitations and model adaptivity create significant obstacles for robust object detection in rainy conditions. Therefore, this work proposes two main approaches: the simulation of realistic rain and new object detection tailored for rainy environments. As illustrated in Fig. 3, we introduce DRET (a), a method that generates more accurate and realistic simulated rain data for detector training. Additionally, we present SRKD (b), a general framework that enhances the detector’s robustness in rainy conditions without compromising efficiency.

### DRET Rain Simulation Method

Rain simulation models take a sunny point cloud data  $D$  as input and generate a simulated rainy point cloud  $D^*$ . Ex-



isting simulation models such as SPRAY [29] and LISA [13] have not considered both the dynamic particle simulation and rainy environment theory in a unified pipeline. We propose a new integrated, two-stage simulation method. As depicted in Fig. 3 (a), its first stage employs the Unity3D engine to simulate dynamic splashing. It also utilizes Perlin noise [35] to replicate wind interference. However, this particle simulation alone doesn't account for LIDAR reflection intensity for rain particles. Thus, we additionally introduce a second stage of performing a scene process following the rainy environment theory [13, 11] to address this limitation.

In the first stage, similar to SPRAY [29], we utilize the particle emitter in the dynamics particle system to simulate water splashes caused by moving vehicles. We incorporate three splash mechanisms: bow wave (BW), side wave (SW), and tread pickup (TP) following SPRAY. But unlike SPRAY, we use Perlin noise to introduce random accelerations along the  $x$ ,  $y$ , and  $z$  axes. This extra design better imitates wind perturbations and contributes to a broader range of realistic rain particle behaviors.

After the initial stage, we obtain sets of rain particles. However, merging them directly into the sunny point clouds, as done in SPRAY, is not a good idea. Because it results in the absence of LiDAR intensity information for rain particles, and the intensity of the original points would remain unadjusted for rainy conditions. Therefore, we introduce an additional scene processing step based on the rainy environ-

ment theory in the second stage.

Before conducting the scene processing, we collect the location, number, inclination and maximum distance parameters of the LiDARs used in the dataset. These parameters are used to establish a correspondence between the point cloud data  $D$  and the rain particle set  $P$ . This gives us matched pairs  $\{(D_i, P_j)\}$ , in which each pair of points originates from the same laser beam reflection.

Next, unlike LISA's random generation of rain particles, we employ more realistic rain particle sets  $P$  for scene processing. We also adopt more accurate formulas from fog simulation [11]. Specifically, for a matched pair  $(D_i, P_j)$ , where  $D_i$  is a point with reflection intensity  $I_i$  and distance  $R_i$ , and  $P_j$  is a rain particle with distance  $R_j$ , we calculate the intensity  $I_j$  of  $P_j$  using

$$I_j = C_A P_0 \beta \int_0^{2\tau_H} \sin^2 \left( \frac{\pi}{2\tau_H} t \right) \frac{\exp \left( -2\alpha \left( R_j - \frac{ct}{2} \right) \right)}{\left( R_j - \frac{ct}{2} \right)^2} \times \gamma \left( R_j - \frac{ct}{2} \right) U \left( R_i - R_j + \frac{ct}{2} \right) dt, \quad (1)$$

where  $R_1, R_2$  are the sensor optical parameters,  $\beta_0$  is the differential reflectance of point,  $\beta$  is the scattering rate,  $\alpha$  is the attenuation coefficient,  $c$  is the speed of light,  $\tau_H$  is the



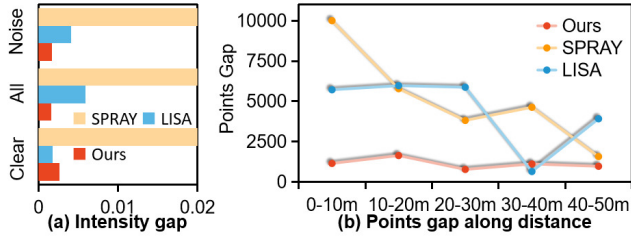


Figure 4: The average intensity gap. (b) The average points gap in each distance interval.

half-power pulse width,  $U$  is the Heaviside function, and

$$C_A P_0 = I_i \frac{R_i^2}{\beta_0}, \gamma(R) = \begin{cases} 0, & R \leq R_1 \\ \frac{R-R_1}{R_2-R_1}, & R_1 < R < R_2 \\ 1, & R_2 \leq R \end{cases} .$$

The calculation is performed using Simpson’s  $1/3$  rule for numerical integration.

After calculating the intensity  $I_j$  of  $P_j$ , we use  $P_j$  to replace  $D_i$  in  $D$  to simulate the occlusion of dense noise in real rain. This process yields a new point cloud  $D'$ . Then, following LISA [13], we adjust the part of original sunny points in  $D'$  to reflect rainy weather conditions. We collect points where the LiDAR received power  $\mathcal{P}$  exceeds the minimum LiDAR received power  $\mathcal{P}_{min}$  to get the simulated rainy point cloud  $D^*$ :

$$D^* = \{D'_i \mid \mathcal{P}_i \geq \mathcal{P}_{min}\}. \quad (2)$$

where  $\mathcal{P}_i = \frac{I_i}{R_i^2}$ ,  $\mathcal{P}_{min} = 0.9R_{max}^2$ , and  $R_{max}$  is the max distance of LiDAR.

**Comparison with other rain simulation methods.** We simulated 10k rainy point cloud data using LISA [13], SPRAY [29], and our DRET method, respectively. We then analyzed the average intensity gap between these simulated data and real rain data (see Fig. 4 (a)). The SPRAY has a serious gap in intensity with the real data, mainly because of the missing rain particle intensity calculations and original clear point corrections, as mentioned earlier. Although LISA seems to have a smaller intensity gap in the clear points this is a fluctuation caused by the randomization of the rain rate parameter. The intensity gap of our method is significantly less than LISA in terms of noise and all points, especially on all points. By analyzing the average points gap along distance (see Fig. 4 (b)), we can also find that SPRAY has a huge gap because it can not filter the low received power points. While LISA has a small points gap at 30-40m, the overall points gap fluctuates greatly and the overall gap is significantly larger than our method. In contrast, our simulated data is smaller in both the intensity gap and points gap, indicating that our method is more realistic.

In summary, our DRET simulation method can offer a lot of realistic simulated rain data, thereby broadening the possibilities for research into robust 3D object detection in rain.

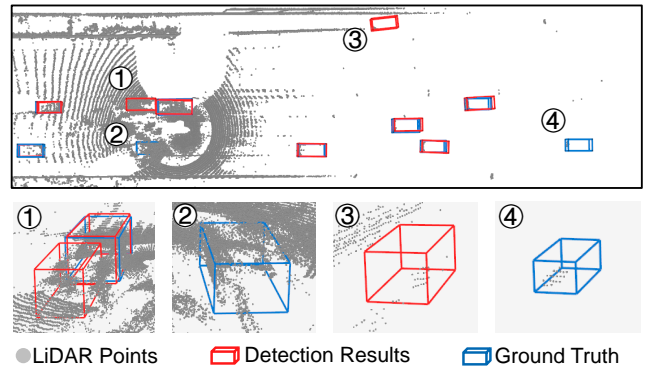


Figure 5: Examples of rainy condition effects on 3D object detection. The blue and red boxes represent groundtruths and predictions.

### Sunny-to-Rainy Knowledge Distillation

Expanding rainy data using DRET as a data augmentation during training is valuable. However, this strategy alone does not address the gaps existing between sunny and rainy data. Even applying distillation techniques as seen in previous works [5, 6, 37] cannot effectively bridge the weather-related gaps. In light of this, we undertake an initial analysis of how these weather disparities impact 3D object detection. Based on these analyses, we design the SRKD framework to overcome the challenges posed by the weather gaps when distilling knowledge from sunny to rainy conditions. As shown in Fig.3 (b), the SRKD framework brings the following technical contributions. Firstly, we devise a knowledge distillation approach capable of facilitating the transition of 3D detectors from sunny to rainy scenarios. This includes the integration of *Adaptively Weighted Instance Distillation (AWID)* and *Precise Response Distillation (PRD)*. Additionally, we introduce *Noise-Aware Prediction Correction (NAPC)* to mitigate the influence of rain-induced noise.

**Analysis on impact of rain on 3D object detection.** As previously discussed, the presence of dense rain noise and the absence of points in rainy conditions pose significant challenges for 3D object detection. Table 1 highlights the substantial decrease in both precision and recall for VoxelRCNN [33] on the WOD dataset during rainy conditions. This effect is further illustrated in Fig. 5, which depicts the impact of rainy weather on the detector’s performance: 1) *Dense rain noise*. The presence of dense rain noise often results in numerous false positives (Fig. 5①). Additionally, these noise induced detections can erode the confidence of predictions, potentially leading to false negatives (Fig.5②). 2) *Missing points*. The sparse clustered background points due to rain induce false positives (Fig.5③). Meanwhile, the absence of foreground points creates sparse point representations for many objects, making them difficult to recall accurately(Fig.5④).

Thus, instead of naively utilizing simulated data as augmentation, it is crucial to propose a novel framework to address the domain gap between rainy and sunny conditions.

Weather	Precision			Recall		
	0.3	0.5	0.7	0.3	0.5	0.7
Sunny	46.8	44.8	34.6	87.3	84.1	69.7
Rainy	33.6	32.3	27.3	83.2	80.0	66.7
Degradation	-13.2	-12.5	-7.3	-4.1	-4.1	-3.0

Table 1: Precision and recall of vehicle in different weather. 0.3, 0.5, and 0.7 are the IoU thresholds.

**AWID.** Distilling sunny instances into rainy instances can help students efficiently extract features from indistinguishable and sparse objects. However, directly distilling instance features from sunny teachers to rainy students, following [5, 6], poses a great challenge due to the gap between sunny and rainy object variations. By comparing and analyzing the data of instances under rainy and sunny conditions, we found that the changes in instances are mainly reflected in differences in density and shape. To overcome this challenge, our proposed AWID utilizes the similarity between corresponding sunny and rainy objects as distillation weights for instance features. Our adaptive weighting reduces the domain gap caused by variations in density and shape under different weather conditions. The similarity weight consists of two components: density similarity and shape similarity. For a groundtruth object box  $B_i$  in sunny and rainy conditions, with point clouds  $PC_i^s$  and  $PC_i^r$  of  $d_i^s$  and  $d_i^r$  points, the density similarity  $\hat{S}_i$  is:

$$\hat{S}_i = \tanh\left(\frac{\min(d_i^s, d_i^r)}{|d_i^s - d_i^r| + \epsilon}\right), \quad (3)$$

$\epsilon = 1e-6$  prevents division by zero. Then calculate the shape similarity  $\tilde{S}_i$  by Chamfer Distance  $d_{CD}$  [36]:

$$\tilde{S}_i = 1 - \tanh(d_{CD}(PC_i^s, PC_i^r)). \quad (4)$$

Combining Eqs.3 and Eqs.4 we obtain the similarity  $S_i$ :

$$S_i = \hat{S}_i \cdot \tilde{S}_i. \quad (5)$$

So we can transfer instance feature knowledge for each box from sunny to rainy by using similarity  $S$  as weight:

$$\mathcal{L}_{ins} = \frac{1}{|B|} \sum_{i \in B} S_i \cdot \mathcal{L}_{sml1}(I_i^s, I_i^r), \quad (6)$$

where  $B$  is the groundtruth boxes;  $I_i$  is the  $i$ -th instance feature, superscript  $s, r$  represent sunny and rainy.

**PRD.** Our AWID greatly aids in sunny-to-rainy knowledge distillation. However, it remains specific to the RoI head in two-stage works and lacks comprehensiveness. And we expect the model to predict consistent results for the same scene on sunny and rainy weather.

To address the remaining challenges, we introduce response distillation as a classical distillation approach [27]. This approach promotes prediction consistency between sunny teachers and rainy students. We focus on the teacher’s output in positions where the confidence exceeds the threshold  $\mathcal{T}$  (0.5), aiming to prevent negative effects from already

difficult sunny objects. Specifically, at estimated foreground positions  $G$ :

$$\mathcal{L}_{cls}^r = \frac{1}{|G|} \sum_{i \in G} \mathbb{I}(\phi(c_i^s) \geq \mathcal{T}) \cdot \mathcal{L}_{mse}(c_i^r, c_i^s), \quad (7)$$

$$\text{and } \mathcal{L}_{reg}^r = \mathcal{L}_{reg}^{3D}(b^r, b^s), \quad (8)$$

where the superscripts  $r$  and  $s$  indicate rainy student and sunny teacher, respectively;  $c$  and  $b$  represent classification and box regression predictions;  $\phi$  is the sigmoid function;  $\mathbb{I}$  filters the teacher’s classification output, focusing on high-confidence predictions;  $\mathcal{L}_{cls}^r$  and  $\mathcal{L}_{reg}^r$  are the classification and regression response distillation losses. By combining Eqs.7 and Eqs.8, the total precise response distillation loss is obtained as:

$$\mathcal{L}_{rsp} = \lambda_1 \mathcal{L}_{cls}^r + \lambda_2 \mathcal{L}_{reg}^r. \quad (9)$$

where set  $\lambda_1 = 15$ ,  $\lambda_2 = 0.2$  according to [27].

**NAPC.** The previous modules improve model robustness in rainy conditions via sunny-to-rainy distillation. However, this implicit processing alone cannot mitigate false positives caused by dense rain noise effectively. The rain noise caused by splashing caused by the high speed movement of vehicle tires is heavily distributed around the instance. We leverage the key advantage of simulated rainy data, which provides self-contained rain noise labels for correcting prediction inaccuracies. We introduce a Noise-Aware Prediction Correction head, NAPC, which focuses on suppressing rain noise. For a predicted box  $B_i$  with  $\mathcal{K}$  points, including  $\hat{\mathcal{K}}$  noise points and  $\tilde{\mathcal{K}}$  non-noise points ( $\hat{\mathcal{K}} + \tilde{\mathcal{K}} = \mathcal{K}$ ), the noise ratio  $\mathcal{R}_i$  is calculated as:

$$\mathcal{R}_i = \frac{\hat{\mathcal{K}}}{\tilde{\mathcal{K}} + \epsilon}, \quad (10)$$

where  $\epsilon = 1e-6$  is a small constant to prevent division by zero. The noise-aware prediction correction loss  $\mathcal{L}_{napc}$  is calculated as:

$$\mathcal{L}_{napc} = \frac{1}{|B|} \sum_{i \in B} \tanh(\mathcal{R}_i) \cdot C_i, \quad (11)$$

where  $B$  represents prediction boxes, and  $C_i$  is the confidence of the  $i$ -th prediction box.

**Overall Loss Function.** We train the rainy student while keeping the pre-trained sunny teacher fixed (see Fig.3) with the following supervision losses and distillation losses:

$$\mathcal{L} = \mathcal{L}_{cls} + \mathcal{L}_{reg} + \eta_1 \mathcal{L}_{ins} + \eta_2 \mathcal{L}_{rsp} + \eta_3 \mathcal{L}_{napc} \quad (12)$$

where  $\mathcal{L}_{cls}$  is classification loss and  $\mathcal{L}_{reg}$  is regression loss;  $\eta_1, \eta_2$  and  $\eta_3$  are hyper-parameters.

## Experiments

We conducted evaluations of our proposed DRET and SRKD on the Waymo Open Dataset (WOD) [34]. To demonstrate the effectiveness of 3D detection under rainy condition, we compared the performance of state-of-the-art model DSVT [10] and PV-RCNN++ [18], Voxel-RCNN [33].

Methods	All(L1) mAP/mAPH	All(L2) mAP/mAPH	Vehicle(L1) mAP/mAPH	Vehicle(L2) mAP/mAPH	Ped.(L1) mAP/mAPH	Ped.(L2) mAP/mAPH
Voxel-RCNN [33]	65.3/62.6	55.8/53.7	73.2/72.8	66.6/66.2	57.4/52.4	45.1/41.1
+ Our DRET-Aug&SRKD	<b>69.5/66.2</b>	<b>60.1/57.3</b>	<b>75.0/74.6</b>	<b>68.5/68.1</b>	<b>63.9/57.8</b>	<b>51.6/46.4</b>
<i>Improvement</i>	+4.2/+3.6	+4.3/+3.6	+1.8/+1.8	+1.9/+1.9	+6.5/+5.4	+6.5/+5.3
PV-RCNN++ [18]	66.2/63.4	56.8/54.5	73.7/73.2	67.1/66.7	58.6/53.5	46.5/42.2
+ Our DRET-Aug&SRKD	<b>69.2/66.5</b>	<b>59.8/57.6</b>	<b>76.7/76.2</b>	<b>69.4/69.0</b>	<b>61.6/56.7</b>	<b>50.1/46.2</b>
<i>Improvement</i>	+3.0/+3.1	+3.0/+3.2	+3.0/+3.0	+2.3/+2.3	+3.0/+3.2	+3.6/+4.0
DSVT [10]	69.3/66.5	60.4/57.9	75.1/74.7	68.4/68.0	63.4/58.3	52.3/47.8
+ Our DRET-Aug&SRKD	<b>72.7/69.7</b>	<b>63.6/61.1</b>	<b>76.8/76.4</b>	<b>70.2/69.8</b>	<b>68.5/63.0</b>	<b>57.0/52.3</b>
<i>Improvement</i>	+3.4/+3.2	+3.2/+3.2	+1.7/+1.7	+1.8/+1.8	+5.1/+4.7	+4.7/+4.5

Table 2: The rainy testing results of 3D detectors within our proposed DRET-Aug and SRKD on the WOD-DA (100% training data). All the results are based on our implementation following the open-source code. The best results are in bold.

Methods	All(L1) mAP/mAPH	All(L2) mAP/mAPH	Vehicle(L1) mAP/mAPH	Vehicle(L2) mAP/mAPH	Ped.(L1) mAP/mAPH	Ped.(L2) mAP/mAPH	Cyc.(L1) mAP/mAPH	Cyc.(L2) mAP/mAPH
Voxel-RCNN	77.3/74.9	70.6/68.4	78.4/77.9	69.8/69.4	80.5/74.7	71.7/66.4	73.1/72.0	70.4/69.3
+ Ours	<b>77.6/75.2</b>	<b>71.0/68.6</b>	<b>78.5/78.0</b>	<b>70.0/69.5</b>	<b>81.0/75.1</b>	<b>72.2/66.7</b>	<b>73.4/72.4</b>	<b>70.7/69.7</b>
PV-RCNN++	77.6/75.0	70.8/68.6	79.1/78.6	70.3/69.9	81.1/75.0	72.5/66.8	72.5/71.4	69.7/69.2
+ Ours	<b>78.1/75.6</b>	<b>71.4/69.0</b>	<b>79.3/78.8</b>	<b>70.6/70.1</b>	<b>81.2/75.2</b>	<b>72.6/66.9</b>	<b>73.7/72.7</b>	<b>70.9/69.9</b>
DSVT	79.5/76.9	73.4/70.9	79.1/78.7	71.3/70.8	82.5/76.2	75.2/69.2	<b>76.9/75.8</b>	73.8/72.8
+ Ours	<b>79.6/77.1</b>	<b>73.7/71.2</b>	<b>79.5/79.0</b>	<b>71.6/71.2</b>	<b>82.6/76.5</b>	<b>75.3/69.5</b>	76.8/75.7	<b>74.1/73.0</b>

Table 3: The sunny testing results of 3D detectors within our proposed DRET-Aug and SRKD on the WOD-P (100% training data). All the results are based on our implementation following the open-source code. The best results are in bold.

**Dataset.** The WOD comprises two subsets: Perception (WOD-P) and Domain Adaptation (WOD-DA). The WOD-P contains  $\sim 158k$  training frames and  $\sim 40k$  validation frames, predominantly sunny conditions (99.4%). We directly use the WOD-P validation for sunny testing. The WOD-DA includes various weather conditions such as foggy, cloudy, and rainy. For our rainy testing, we selected  $\sim 3k$  rainy frames for rainy testing. The training process of all models used only the training set of WOD-P.

**Metrics.** The official metrics of WOD are mean Average Precision (mAP(L1), mAP(L2)) with Heading (mAPH(L1), mAPH(L2)), where L1 and L2 denote the difficulty level. Additionally, for the WOD-DA, only vehicle and pedestrian classes have labeled annotations for evaluation.

**Implementation and training details.** We trained models using two LiDAR returns and a single frame. The specific implementation and training details for each baseline are provided in the supplementary material. In the DRET, we used atmospheric parameters following [11] and [13]. In the SRKD framework, we set the hyper-parameters  $\eta_1$ ,  $\eta_2$ , and  $\eta_3$  (eq.12) as 2.0, 0.5, and 2.0.

## Main Experiment Results

We conducted three model comparison groups. The models were trained on the WOD-P training set based on DRET augmentation (DRET-Aug) and evaluated on the WOD-P validation set and the rainy data of the WOD-DA.

**Performance comparison under rainy weather.** We first evaluated rainy performance on the WOD-DA. Table 2

shows our proposed DRET-Aug and SRKD significantly improve the performance of all 3D detectors in rain. With the SRKD training using DRET-Aug augmentation, Voxel-RCNN, PV-RCNN++, and DSVT achieved improvements of 4.3%, 3.0%, and 3.2% on All(L2-mAP), respectively. Notably, all detectors show substantial gains in the pedestrian class, particularly Voxel-RCNN with a remarkable improvement of 6.5% on Ped.(L2-mAP). This demonstrates the capability of our framework to improve challenging small object detection under rainy conditions. The results demonstrate the effectiveness and broad applicability of our design.

**Performance comparison under sunny weather.** In contrast to existing methods [31, 25] that only focus on performance under adverse weather, it is also essential to maintain performance in sunny weather. Table 3 demonstrates that our framework also slightly improves the performance of 3D detectors in sunny conditions. The performance gains mainly come from the enhanced robustness to handle sparse and indistinguishable objects.

**Rain simulation methods.** In Table 4, we further compared our DRET with the leading rain simulation methods, LISA-Aug and SPRAY-Aug. We observed that plain rain data augmentation alone does not provide significant improvement, as mentioned earlier. Although SPRAY-Aug achieves the best performance on All(L1-mAP), slightly outperforming our DRET-Aug. However, combining all metrics, our method still performs better, especially at the more comprehensive L2 difficulty. Additionally, our DRET-Aug achieves an improvement of 0.5% and 0.6% on All(L2-mAP) compared to LISA-Aug and SPRAY-Aug. These re-

Methods	All(L1) mAP/mAPH	All(L2) mAP/mAPH
Baseline	65.3/62.6	55.8/53.7
+ LISA-Aug [13]	65.5/63.2	56.1/54.3
+ SPRAY-Aug [29]	<b>66.0/63.0</b>	56.0/53.9
+ DRET-Aug (Ours)	65.9/ <b>63.4</b>	<b>56.6/54.7</b>

Table 4: Comparison with state-of-the-art rain simulation methods on the WOD-DA.(100% training data).

Methods	All(L1) mAP/mAPH	All(L2) mAP/mAPH
Baseline	65.3/62.6	55.8/53.7
+ De-Noising [7]	66.9/64.1	56.1/55.4
+ SPG [28]	67.5/64.7	58.0/55.9
+ SRKD (Ours)	<b>69.5/66.2</b>	<b>60.1/57.3</b>

Table 5: Comparison with state-of-the-art 3D object detection in rain methods on the WOD-DA. (100% training data).

Methods	All(L1) mAP/mAPH	All(L2) mAP/mAPH
Voxel-RCNN [33]	65.3/62.6	55.8/53.7
+ Our DRET-Aug	<b>65.9/63.4</b>	<b>56.6/54.7</b>
PV-RCNN++ [18]	66.2/63.4	56.8/54.5
+ Our DRET-Aug	<b>67.0/64.1</b>	<b>57.8/55.4</b>
DSVT [10]	69.3/66.5	60.4/57.9
+ Our DRET-Aug	<b>69.9/67.3</b>	<b>61.0/58.7</b>

Table 6: The rainy testing results of 3D detectors with our proposed DRET-Aug on the WOD-DA (100% training data).

sults again prove DRET’s realism by analyzing the rainy performance gained from simulated data.

**Robust 3D object detection methods in rain.** Given the limited prior work on 3D object detection under rainy conditions, we compared our method to the de-noising [7] and SPG [28]. As shown in Table 5, our SRKD has improved by 4.0% and 2.1% All(L2-mAP) respectively compared to De-Noising and SPG.

### Ablation Study

**Data augmentation based on DRET-Aug.** To further explore the improvements achieved solely by our DRET-Aug data augmentation, we trained the above baseline 3D detectors with DRET-Aug alone. As shown in Table 6, DRET-Aug improves Voxel-RCNN, PV-RCNN++ and DSVT by 0.8%, 1.0% and 0.6% on All(L2-mAP), respectively.

**Component of SRKD analysis.** Furthermore, to validate the efficacy of each component in our proposed SRKD, we conducted an ablation study using 20% training data. The baseline model used is Voxel-RCNN [33] trained with our DRET-Aug. As shown in Table 7, the inclusion of our proposed components AWID, PRD, and NAPC significantly improves the performance of the Voxel-RCNN baseline.

Method	AWID	PRD	NAPC	All(L1) mAP/mAPH
Voxel-RCNN	✓			63.3/60.7
	✓	✓		65.3/62.7
	✓	✓	✓	<b>66.9/64.2</b>

Table 7: Effects of the different components of SRKD.

Method	$\hat{S}$	$\tilde{S}$	All(L1) mAP/mAPH
Voxel-RCNN + AWID			62.8/60.2
	✓		64.0/61.4
	✓	✓	<b>65.3/62.7</b>

Table 8: Effects of the different weighting strategy.

Specifically, AWID, PRD, and NAPC yield gains of 2.0%, 0.9%, and 0.7% on All(L1-mAP), respectively. This highlights the effectiveness of our SRKD components.

**Similarity weighting strategies.** Finally, we tested the different weighting strategies in our AWID module using shape ( $\hat{S}$ ) and density ( $\tilde{S}$ ) similarity. As shown in Table 8, directly distilling rainy-sunny instance features without any weighting performs poorly. This confirms that it is not reasonable to distill all instances equally. Moreover, using both  $\hat{S}$  and  $\tilde{S}$  as weighting strategies yields the best performance, improving upon the no weighting strategy by 2.5% on All (L1-mAP). This validates the importance of our designed adaptive weighting for distilling instance features.

## Conclusion

We propose a novel design including DRET and SRKD for 3D detection in sunny and rainy conditions. It uses DRET, a realistic rain simulation, to generate rainy data and mitigate data scarcity. Our SRKD framework then transfers sunny knowledge to rainy detectors via sunny-to-rainy knowledge distillation. Sufficient experimental results of the WOD show that our design can enhance the robustness of 3D detectors in rain. Moreover, our design can even slightly improve the sunny performance of 3D detectors.

**Limitations.** Our two-stage DRET requires preprocessing to generate particle sets and cannot be end-to-end. While inference efficiency is unchanged, training time increases unavoidably mainly due to shape similarity calculation.

## Acknowledgements

This work was supported in part by the National Natural Science Foundation of China (No.62171393), and the Fundamental Research Funds for the Central Universities (No.20720220064).

## SRKD: Supplementary Material

### Detailed Visualization of Real Rainy Point Clouds

The main paper mentions *dense rain noise* and *missing points* two critical phenomena in rainy point clouds. In order to understand these two phenomena more obviously, we visualize three rainy point clouds in WOD-DA as shown in Fig. 6. Meanwhile, we box the region where the *dense rain noise* occurs in orange and the region where the *missing points* occurs in purple.

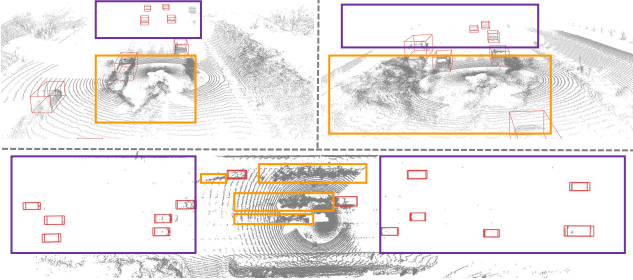


Figure 6: Visualizations of three real rainy day point clouds. Orange is the region where dense rain noise appears, purple is the region where vanishing points appear.

### Detailed Analysis of Performance Improvement

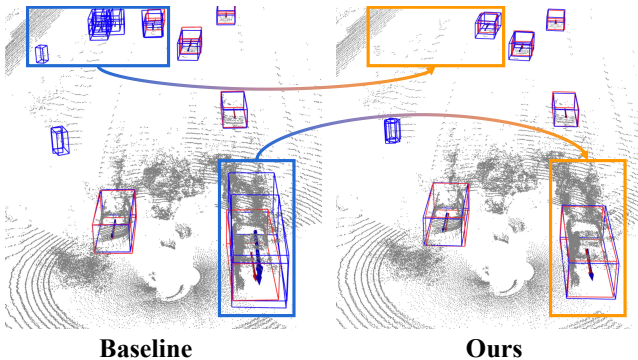


Figure 7: Visualization comparison of detection results in rain. Red boxes indicate groundtruth, and blue boxes indicate test results.

As discussed previously in the main paper, rainy conditions significantly decrease the accuracy and recall of 3D detectors. To investigate whether our proposed DRET-Aug and SRKD methods solve this issue, we conducted the same testing as Table 1 in paper on Voxel-RCNN using our proposed method. The results in Table 9 show that using the proposed DRET-Aug and SRKD leads to significant improvements across all metrics at various IoU thresholds. Specifically, DRET-Aug and SRKD improve Voxel-RCNN 5.6% in precision and 2.9% in recall while the IoU threshold is 0.5 and 0.7, respectively. These experiments demonstrate that our DRET-Aug and SRKD effectively reduce the false positives and negatives that enhance 3D object detection in rain.

This result can likewise be further observed in Fig. 7, where it can be found that the robustness of the baseline 3D detector in rain is significantly enhanced by adding our method.

Method	Precision			Recall		
	0.3	0.5	0.7	0.3	0.5	0.7
Voxel-RCNN	33.6	32.3	27.3	83.2	80.0	66.7
+Ours	38.0	36.7	30.9	85.8	82.1	69.6
<i>Improvement</i>	+5.6	+4.3	+3.6	+2.6	+2.1	+2.9

Table 9: Comparison of vehicle precision and recall under rainy weather. 0.3, 0.5, and 0.7 are the IoU thresholds.

Table 9 in shows the precision and recall improvements by our method, intended to echo our motivation. Following the reviewer’s suggestion, we also conducted more detailed ablation studies to further demonstrate the effectiveness of AWID and NAPC. The results are shown below (20% training data, *IoU* threshold is 0.3):

Model	FP	Precision	Model	FN	Recall
Voxel-RCNN	70.5k	31.9	Voxel-RCNN	8.1k	82.0
+ Our NAPC	57.8k	37.1	+ Our AWID	7.2k	84.6
<i>Improvement</i>	↓18.0%	↑5.2	<i>Improvement</i>	↓11.1%	↑2.6

### Implementation and Training Details

Student	Teacher	GPUs	Total Batchsize	Sync_BN	Epoch
Voxel-RCNN	Voxel-RCNN	4×RTX 3090	4×6=24	✗	40
PV-RCNN++	PV-RCNN++	4×RTX 3090	4×4=16	✗	40
DSVT	DSVT	6×RTX 3090	6×3=18	✓	30

Table 10: Implementation and training details of three 3D detectors with our DRET-Aug and SRKD.

Table 10 is a detailed supplement to the main paper experimental implementation and training details. The code implementation is based on the open-source code of the corresponding 3D detector in the OpenPCDet project. Additionally, the rest of the training details are shown in Table 10.

### Computational and Memory Cost

We tested the single-stage DSVT and the two-stage PV-RCNN++. Below, we present the computational and memory costs incurred during the **training phase**.

Model	Training time	Memory
DSVT	49h	21G
+ Our SRKD	61h	23G
Cost of SRKD in DSVT	↑24%	↑10%
PV-RCNN++	54h	21G
+ Our SRKD	83h	24G
Cost of SRKD in PV-RCNN++	↑54%	↑14%

The results indicate our SRKD method does incur additional computational and memory costs, but the extra costs are not substantial because the teacher model does not require gradient computation and memory optimization. Furthermore, during the **inference phase**, as we only use the student model and do not calculate the loss, there are no additional computational and memory costs.



## References

- [1] Z. Yang, Y. Sun, S. Liu, and J. Jia, "3DSSD: Point-Based 3D Single Stage Object Detector," in *CVPR*, 2020.
- [2] X. Huang, P. Wang, X. Cheng, D. Zhou, Q. Geng, and R. Yang, "The ApolloScape Open Dataset for Autonomous Driving and its Application," *IEEE Trans. Pattern Anal. Mach. Intell.*, vol. 42, 2020.
- [3] C. A. Diaz-Ruiz, Y. Xia, Y. You, J. Nino, J. Chen, J. Monica, X. Chen, K. Luo, Y. Wang, M. Emond, W.-L. Chao, B. Hariharan, K. Q. Weinberger, and M. Campbell, "Ithaca365: Dataset and Driving Perception Under Repeated and Challenging Weather Conditions," in *CVPR*, 2022.
- [4] M. Pitropov, D. Garcia, J. Rebello, M. Smart, C. Wang, K. Czarnecki, and S. Waslander, "Canadian Adverse Driving Conditions Dataset," *The International Journal of Robotics Research*, vol. 40, 2021.
- [5] W. Zheng, M. Hong, L. Jiang, and C.-W. Fu, "Boosting 3D Object Detection by Simulating Multimodality on Point Clouds," in *CVPR*, 2022.
- [6] W. Zheng, L. Jiang, F. Lu, Y. Ye, and C.-W. Fu, "Boosting Single-Frame 3D Object Detection by Simulating Multi-Frame Point Clouds," in *ACMMM*, 2022.
- [7] R. Heinzler, F. Piewak, P. Schindler, and W. Stork, "CNN-Based Lidar Point Cloud De-Noising in Adverse Weather," *IEEE Robotics and Automation Letters*, vol. 5, 2020.
- [8] H. Sheng, S. Cai, Y. Liu, B. Deng, J. Huang, X.-S. Hua, and M.-J. Zhao, "Improving 3D Object Detection With Channel-Wise Transformer," in *ICCV*, 2021.
- [9] N. Charron, S. Phillips, and S. L. Waslander, "De-noising of Lidar Point Clouds Corrupted by Snowfall," in *CRV*, 2018.
- [10] H. Wang, C. Shi, S. Shi, M. Lei, S. Wang, D. He, B. Schiele, and L. Wang, "DSVT: Dynamic Sparse Voxel Transformer With Rotated Sets," in *CVPR*, 2023.
- [11] M. Hahner, C. Sakaridis, D. Dai, and L. Van Gool, "Fog Simulation on Real LiDAR Point Clouds for 3D Object Detection in Adverse Weather," in *ICCV*, 2021.
- [12] Y. Zhang, Q. Hu, G. Xu, Y. Ma, J. Wan, and Y. Guo, "Not All Points Are Equal: Learning Highly Efficient Point-Based Detectors for 3D LiDAR Point Clouds," in *CVPR*, 2022.
- [13] V. Kilic, D. Hegde, V. A. Sindagi, A. Cooper, M. Foster, and V. M. Patel, "Lidar Light Scattering Augmentation (LISA): Physics-based Simulation of Adverse Weather Conditions for 3D Object Detection," *ArXiv*, 2021.
- [14] A. Piroli, V. Dallabetta, M. Walessa, D. Meissner, J. Kopp, and K. Dietmayer, "Robust 3D Object Detection in Cold Weather Conditions," in *2022 IEEE Intelligent Vehicles Symposium (IV)*, 2022.
- [15] A. H. Lang, S. Vora, H. Caesar, L. Zhou, J. Yang, and O. Beijbom, "PointPillars: Fast Encoders for Object Detection From Point Clouds," in *CVPR*, 2019.
- [16] S. Shi, X. Wang, and H. Li, "PointRCNN: 3D Object Proposal Generation and Detection From Point Cloud," in *CVPR*, 2019.
- [17] S. Shi, C. Guo, L. Jiang, Z. Wang, J. Shi, X. Wang, and H. Li, "PV-RCNN: Point-Voxel Feature Set Abstraction for 3D Object Detection," in *CVPR*, 2020.
- [18] S. Shi, L. Jiang, J. Deng, Z. Wang, C. Guo, J. Shi, X. Wang, and H. Li, "PV-RCNN++: Point-Voxel Feature Set Abstraction With Local Vector Representation for 3D Object Detection," *Int. J. Comput. Vision*, vol. 131, 2022.
- [19] C. He, H. Zeng, J. Huang, X.-S. Hua, and L. Zhang, "Structure Aware Single-Stage 3D Object Detection From Point Cloud," in *CVPR*, 2020.
- [20] Y. Yan, Y. Mao, and B. Li, "SECOND: Sparsely Embedded Convolutional Detection," *Sensors*, vol. 18, 2018.
- [21] W. Zheng, W. Tang, L. Jiang, and C.-W. Fu, "SE-SSD: Self-Ensembling Single-Stage Object Detector From Point Cloud," in *CVPR*, 2021.
- [22] X. Wu, L. Peng, H. Yang, L. Xie, C. Huang, C. Deng, H. Liu, and D. Cai, "Sparse Fuse Dense: Towards High Quality 3D Detection with Depth Completion," in *CVPR*, 2022.
- [23] S. Teufel, G. Volk, A. Von Bernuth, and O. Bringmann, "Simulating Realistic Rain, Snow, and Fog Variations For Comprehensive Performance Characterization of LiDAR Perception," in *2022 IEEE 95th Vehicular Technology Conference: (VTC2022-Spring)*, 2022.
- [24] N. A. M. Mai, P. Duthon, L. Khoudour, A. Crouzil, and S. A. Velastin, "3D Object Detection with SLS-Fusion Network in Foggy Weather Conditions," *Sensors*, vol. 21, 2021.
- [25] J. Lin, H. Yin, J. Yan, W. Ge, H. Zhang, and G. Rigoll, "Improved 3D Object Detector Under Snowfall Weather Condition Based on LiDAR Point Cloud," *IEEE Sensors Journal*, vol. 22, 2022.
- [26] M. Hahner, C. Sakaridis, M. Bijelic, F. Heide, F. Yu, D. Dai, and L. Van Gool, "LiDAR Snowfall Simulation for Robust 3D Object Detection," in *CVPR*, 2022.
- [27] J. Yang, S. Shi, R. Ding, Z. Wang, and X. Qi, "Towards Efficient 3D Object Detection with Knowledge Distillation," *NIPS*, vol. 35, 2022.
- [28] Q. Xu, Y. Zhou, W. Wang, C. R. Qi, and D. Anguelov, "SPG: Unsupervised Domain Adaptation for 3D Object Detection via Semantic Point Generation," in *ICCV*, 2021.
- [29] Y.-C. Shih, W.-H. Liao, W.-C. Lin, S.-K. Wong, and C.-C. Wang, "Reconstruction and Synthesis of Lidar Point Clouds of Spray," *IEEE Robotics and Automation Letters*, vol. 7, 2022.
- [30] Z. Yang, Y. Sun, S. Liu, X. Shen, and J. Jia, "STD: Sparse-to-Dense 3D Object Detector for Point Cloud," in *ICCV*, 2019.
- [31] M. Bijelic, T. Gruber, F. Mannan, F. Kraus, W. Ritter, K. Dietmayer, and F. Heide, "Seeing Through Fog

Without Seeing Fog: Deep Multimodal Sensor Fusion in Unseen Adverse Weather,” in *CVPR*, 2020.

- [32] H. Wu, C. Wen, S. Shi, X. Li, and C. Wang, “Virtual Sparse Convolution for Multimodal 3D Object Detection,” in *CVPR*, 2023.
- [33] J. Deng, S. Shi, P. Li, W. Zhou, Y. Zhang, and H. Li, “Voxel R-CNN: Towards High Performance Voxel-based 3D Object Detection,” *AAAI*, vol. 35, 2021.
- [34] P. Sun, H. Kretzschmar, X. Dotiwalla, A. Chouard, V. Patnaik, P. Tsui, J. Guo, Y. Zhou, Y. Chai, B. Caine, V. Vasudevan, W. Han, J. Ngiam, H. Zhao, A. Timofeev, S. Ettinger, M. Krivokon, A. Gao, A. Joshi, Y. Zhang, J. Shlens, Z. Chen, and D. Anguelov, “Scalability in Perception for Autonomous Driving: Waymo Open Dataset,” in *CVPR*, 2020.
- [35] R. Bridson, J. Houriham, and M. Nordenstam, “Curl-noise for procedural fluid flow,” *ACM Trans. Graph.*, vol. 26, no. 3, p. 46–es, jul 2007. [Online]. Available: <https://doi.org/10.1145/1276377.1276435>
- [36] G. Borgefors, “Distance transformations in digital images,” *Computer vision, graphics, and image processing*, vol. 34, no. 3, pp. 344–371, 1986.
- [37] A. T. Do and M. Yoo, “Losdistillnet: 3d object detection in point cloud under harsh weather conditions,” *IEEE Access*, vol. 10, pp. 84 882–84 893, 2022.
- [38] Q. Hu, B. Yang, L. Xie, S. Rosa, Y. Guo, Z. Wang, N. Trigoni, and A. Markham, “Randla-net: Efficient semantic segmentation of large-scale point clouds,” in *Proceedings of the IEEE/CVF conference on computer vision and pattern recognition*, 2020, pp. 11 108–11 117.